



## Review

## Wave climate projections along the French coastline: Dynamical versus statistical downscaling methods

Amélie Laugel <sup>a,b,\*</sup>, Melisa Menendez <sup>c</sup>, Michel Benoit <sup>a,b</sup>, Giovanni Mattarolo <sup>a,b</sup>, Fernando Méndez <sup>c</sup><sup>a</sup> Saint-Venant Hydraulics Laboratory, Université Paris-Est (EDF R&D, Cerema, Ecole des Ponts ParisTech), Chatou, France<sup>b</sup> National Hydraulic and Environment Laboratory (LNHE), EDF R&D, Chatou, France<sup>c</sup> Environmental Hydraulics Institute, "IH-Cantabria", Universidad de Cantabria, Santander, Spain

## ARTICLE INFO

## Article history:

Received 7 October 2013

Received in revised form 2 September 2014

Accepted 6 September 2014

Available online 28 September 2014

## Keywords:

Wave climate

Wave modeling

Statistical downscaling

Dynamical downscaling

Weather types

Climate change

## ABSTRACT

The estimation of possible impacts related to climate change on the wave climate is subject to several levels of uncertainty. In this work, we focus on the uncertainties inherent in the method applied to project the wave climate using atmospheric simulations. Two approaches are commonly used to obtain the regional wave climate: dynamical and statistical downscaling from atmospheric data. We apply both approaches based on the outputs of a global climate model (GCM), ARPEGE-CLIMAT, under three possible future scenarios (B1, A1B and A2) of the Fourth Assessment Report, AR4 (IPCC, 2007), along the French coast and evaluate their results for the wave climate with a high level of precision. The performance of the dynamical and the statistical methods is determined through a comparative analysis of the estimated means, standard deviations and monthly quantile distributions of significant wave heights, the joint probability distributions of wave parameters and seasonal and interannual variability. Analysis of the results shows that the statistical projections are able to reproduce the wave climatology as well as the dynamical projections, with some deficiencies being observed in the summer and for the upper tail of the significant wave height. In addition, with its low computational time requirements, the statistical downscaling method allows an ensemble of simulations to be calculated faster than the dynamical method. It then becomes possible to quantify the uncertainties associated with the choice of the GCM or the socio-economic scenarios, which will improve estimates of the impact of wave climate change along the French coast.

© 2014 Elsevier Ltd. All rights reserved.

## Contents

1. Introduction . . . . .	36
2. Atmospheric datasets . . . . .	37
3. Presentation of the dynamical and the statistical methods . . . . .	37
3.1. The dynamical downscaling (DD) method . . . . .	37
3.2. The statistical downscaling (SD) method . . . . .	38
3.2.1. Predictor definition . . . . .	38
3.2.2. Predictor classification . . . . .	39
3.2.3. Regression model . . . . .	41
3.2.4. Wave projection . . . . .	42
3.3. Metrics for comparing the SD vs. the DD method . . . . .	42
4. Results from the dynamical and the statistical downscaling methods . . . . .	43
4.1. Annual climatology . . . . .	43
4.2. Seasonal variability . . . . .	44
4.3. Interannual variability . . . . .	47

\* Corresponding author at: Saint-Venant Hydraulics Laboratory, Université Paris-Est (EDF R&D, Cerema, Ecole des Ponts ParisTech), Chatou, France. Tel.: +33 1 30 87 72 01; fax: +33 1 30 87 80 86.

E-mail address: [amelie.laugel@gmail.com](mailto:amelie.laugel@gmail.com) (A. Laugel).

5. Discussions and conclusion .....	48
Acknowledgments .....	49
Appendix A. Validation of the DD and the SD methods for the present climate. ....	49
References .....	49

---

## 1. Introduction

An improved understanding of the present and future wave climatology is necessary for numerous marine and coastal activities, such as offshore industries, the assessment of flooding risk, the design of maritime structures and the evaluation of wave energy resources. Analysis of the impacts of climate change on waves or other met-ocean phenomena, such as wind and pressure patterns, sea level rise, storm surges or the evolution of coastal erosion, requires knowledge of the variability of these phenomena and estimation of the uncertainties inherent to the global climate models (GCMs), scenarios and methods applied to project these variables. There are two main methods used to simulate wave conditions from meteorological outputs: dynamical downscaling (DD) and statistical downscaling (SD). The DD method, based on third-generation dynamical wave models driven by 10 m wind fields, continuously simulates wave parameters over an oceanic or coastal domain using a detailed physical approach. On the other hand, the SD method, based on the definition of a statistical relationship between a local sea state referred to as the “predictand” and an atmospheric “predictor”, such as sea level pressure, simulates local wave parameters and requires little computational time. Within the context of estimating the impact of climate change on the future wave climate, both methods are already well developed and have been put into practice. In addition, comparison of these methods regarding regional wave projections is a key point for estimating the uncertainties associated with studies on climate change.

The initial efforts to project the future wave climate have focused on global projections with dynamical (Mori et al., 2010; Hemer et al., 2013a) and statistical simulations (Wang et al., 2004; Wang and Swail, 2006; Mori et al., 2013). At a global scale, recent DD studies have agreed upon a latitudinal structure of significant wave height (SWH) evolution at the end of the XXIst century, characterized by a decrease of future mean wave heights in North middle latitudes and an increase of the mean SWH in the Antarctic Ocean and in equatorial areas for some models. Mori et al. (2010) provided global simulations of the future mean and extreme wave climate (SWH) in response to the A1B scenario throughout a GCM developed by the Japanese Meteorological Research Institute and Japan Meteorological Agency. They reported a projected decrease of the mean SWH of approximately 7% in the North Atlantic for the period from 2075–2100. Hemer et al. (2013a) compared the dynamical SWH projections of the ECHAM5 and CSIRO Mk3.5 GCMs for the A2 scenario (period 2070–2099) and observed a maximum decrease of the SWH in the central North Atlantic of up to 0.7 m (~15%) with a well-defined seasonal dependence, with a ~1 m decrease occurring in winter and a ~0.2 m decrease in summer. The SWH results were consistent with future weakening of the annual wind speed in the North Atlantic basin, which is predicted to decrease by approximately 3 m/s according to both GCMs but also with a significant decrease in the annual mean wave period (~0.5 s).

Most of the recent studies focusing on regional projections of the wave climate have generally agreed regarding projections of the future mean value of the SWH, whereas their results have diverged for high percentiles of the SWH. Along the French coast, Morellato et al. (1960) applied the DD of ECHAM5 calibrated

against an ERA-40 wind field reanalysis for the B1, A1B and A2 scenarios over the northeast Atlantic. They observed an increase in the mean SWH in the North Sea and a decrease along the French Atlantic coastline, while the future extreme SWH up to the 95th percentile rose for both areas. In the Bay of Biscay, Charles et al. (2012) obtained similar results regarding the evolution of the mean SWH and opposite results for the 95th percentile.

To address the uncertainties associated with wave climate projections, a multi-model approach is needed. However, only a few studies present an ensemble of simulations from several models or scenarios. Weisse et al. (2008) simulated four datasets of wave and surge projections over the northeast Atlantic for the period from 2071–2100 applying the DD of the HadAM3H and ECHAM5 GCMs coupled with the regional model RCAO (Rossby Center Regional Atmosphere–Ocean Model) for the A2 and B2 scenarios. These authors showed that choice of GCM clearly affected the obtained magnitude and spatial patterns of SWH evolution. Then, Hemer et al. (2013b), as coordinators of the COWCLIP community (Coordinate Ocean Wave Climate Project, [www.jcomm.info/cowclip](http://www.jcomm.info/cowclip)) worked to combine the efforts aimed at global wave climate projections. For example, they compared the magnitudes of changes in the SWH indicated by independent dynamical (Mori et al., 2010; Semedo et al., 2013; Hemer et al., 2013a) and statistical wave projections (Wang and Swail, 2006), and they found that 25.8% (7.1%) of global areas are robustly characterized by an annual decrease (increase) in the mean SWH value. The Southern Ocean and some Pacific locations will suffer an increase in the SWH over the last decades of the XXIst century, while North Atlantic middle latitudes will be characterized by a decrease of approximately 5% to 10% of the mean value of the SWH depending on the season and the region. Throughout this comparison, the COWCLIP community also suggested that the downscaling methodology may produce greater uncertainties than climate models or scenarios (Hemer et al., 2013b).

In this context, applying the SD method for wave climate projections is necessary. First, comparison of dynamical and statistical wave projections allows the estimation of uncertainties inherent to the downscaling approach. Second, using an ensemble of SD simulations from different GCMs is a coherent way to define future sea states and estimate some of the uncertainties associated with the choice of a GCM or scenario. Similar to the DD method, the SD method is already well developed and has been put into practice at regional or global scales to increase our global understanding of wave climate evolution. Moreover, its low computation time and required storage capacity promote its use as a real alternative for wave climate projections.

Basically, the statistical downscaling method is conducted by means of regression models, either using a weather pattern-based approach or not. For example, Mori et al. (2013) set up a global statistical regression between wind fields and wave heights through the least squares method, including a distant swell effect correction. They found that future changes in winds and waves clearly depend on the scenario applied, although they showed a similar spatial distribution. The SD method based on weather patterns links the predictand (i.e., local wave characteristics) to particular synoptic-scale weather types (predictor). This approach has been widely used to downscale surface atmospheric variables, such as precipitation or snow (Wilby et al., 2004; Boé et al., 2009;

Tisseuil et al., 2010), and has been successfully applied to project the surface wind field (Najac et al., 2008) or wave height (Espejo et al., 2014). For example, Izaguirre et al. (2012) classified monthly SLP fields and analyzed the links between weather types and the interannual variability of extreme SWHs by means of a time-dependent generalized extreme value (GEV) distribution.

Furthermore, only a few studies have analyzed dynamical versus statistical methods for wave climate projections. Wang et al. (2010) compared these two methods for the present period using ERA-40 wave data. They found that the SD method is more robust than the DD method for the reproduction of seasonal means and extremes. This result is partially explained by the model bias, which is conserved using the DD method, whereas it can be diminished through standardization of the predictor using the SD method. Graham et al. (2013) also applied the SD and DD methods to analyze seasonal extreme SWHs in the North Pacific Ocean. The two methods produced the same pattern of SWH decreases south of 40°N, though the SD method tended to underestimate the magnitude of these changes. In summary, the quality of the obtained wave projection is subject to the quality of the method applied, which must be previously validated. This leads to additional levels of uncertainty associated with the parameterization or calibration of each method, including the wind input calibration, the source and sink term formulations for the spectral wave model and the definition and classification of the predictor.

Within the overall objective of estimating the impact of climate change on the future wave climate along the French coast, this study aims to evaluate the performance of the SD method with respect to the DD method. The DD method, as a deterministic simulation method, is better at accounting for the complex processes of wave propagation, whereas the SD requires additional hypotheses. Therefore, though the input data affect the quality of the projections, the results of the DD method are considered as reference data in this work. We have analyzed 110 grid points distributed along the Atlantic, English Channel and North Sea coastlines of France (inset of Fig. 2) to project the wave climate over the period from 2061–2100. To reduce some levels of uncertainty, the two state-of-the-art methods applied have been previously calibrated and validated, and a specific GCM is used to provide forcing in both approaches. This paper is organized as follows: Section 2 presents the atmospheric data used in this study, and Section 3 describes both the DD and SD methods and the metrics applied to compare them. Then, Section 4 exposes the results, and finally, conclusions and a discussion are presented in Section 5.

## 2. Atmospheric datasets

Waves are generated through the disturbance of wind fields on the sea surface. Consequently, waves in the ocean are simulated using atmospheric information, which can differ depending on the method applied. For example, the DD method requires wind fields with a high spatial and temporal resolution to reproduce wave dynamics, while the SD method requires the best weather conditions (predictor) to define a robust statistical relationship between the predictor and the waves (predictand).

**Table 1**

Characteristics of the meteorological data used as input forcings under the DD and the SD methods.

	ARPEGE-CLIMAT U10 (DD)	ARPEGE-CLIMAT SLP (SD)	CFSR U10 (DD)	CFSR SLP (SD)
Present period	1961–2000 (REF)	1961–2000 (REF)	1979–2009	1979–2009 (learning period)
Future period	2061–2100 (B1, A1B, A2)	2061–2100 (B1, A1B, A2)	–	–
Spatial resolution	0.5° × 0.5°	2.5° × 2.5°	0.312° × 0.312°	2.5° × 2.5°
Temporal resolution	6-h	3-day averaged	1-h	3-day averaged
Predictor area	Atlantic Ocean	North-East Atlantic Ocean	Atlantic Ocean	North-East Atlantic Ocean

In this study, both methods are applied, and two atmospheric variables are used to project the wave climate. Wind fields (U10) are the direct input into the numerical wave model under the DD method, and sea level pressure (SLP) fields characterize synoptic weather conditions under the SD method. First, SLP data from the Climate Forecast System Reanalysis (CFSR) database (Saha et al., 2010) are used in the SD approach to classify atmospheric circulation patterns during current conditions. Global SLPs from the CFSR are available with an hourly temporal resolution and a spatial resolution of 0.5° × 0.5°. However, they are applied here with a 2.5° × 2.5° resolution and a 3-day averaged resolution over the period from 1979–2009. Then, GCMs are used as unique source of atmospheric information to obtain wave climate projections. Here, the GCM ARPEGE-CLIMAT from Météo-France (Salas-Mélia et al., 2005) is employed to project the future wave climate through the application of both DD and SD methods. The ARPEGE-CLIMAT wind and SLP fields have a 6-h resolution and cover a stretched grid centered in the Mediterranean Sea, where the spatial resolution is 0.1° × 0.5°. This spatial resolution increases progressively, reaching approximately 0.5° × 0.5° in the northeast Atlantic. Four runs are available for the ARPEGE-CLIMAT model: one run for the present climate conditions (time period 1961–2000), and three runs, from 2061–2100, associated with future scenarios of the IPCC Fourth Assessment Report, AR4 (IPCC, 2007), (B1, A1B and A2, which are optimistic, intermediate and pessimistic climate scenarios, respectively). Table 1 summarizes the input data used to apply both methods in terms of the resolution, time slice and area.

## 3. Presentation of the dynamical and the statistical methods

A flowchart of the applied methodologies is shown in Fig. 1. An atmospheric input (U10 or SLP) is required to obtain the wave climate under the DD and the SD methods, but the set-ups of the two methods are completely different. The spatial domain configuration, bathymetry and the source terms of the wave numerical model must be fixed under the DD method, while the SD method requires the definition of a robust statistical relationship between the predictand and the predictor. Here, this link is based on a synoptic weather type classification. Finally, the outcomes of the applied methods are compared, not only in terms of the resulting wave climatology but also in terms of the seasonal and interannual wave climate variations. In this study, to compare the DD and the SD methods in a coherent way, an initial validation step was applied to both methods for the present climate using CFSR input data (cf Appendix A). Then, to estimate the future wave climate, both methods were applied over a recent time slice (1961–2000) and a future time slice (2061–2100) using the ARPEGE-CLIMAT database.

### 3.1. The dynamical downscaling (DD) method

The DD method continuously runs a spectral wave model driven by wind fields from GCM simulations during a target period (2061–2100 here). The simulation is deterministic, in the sense that the wave model simulates the time series of sea states at each node

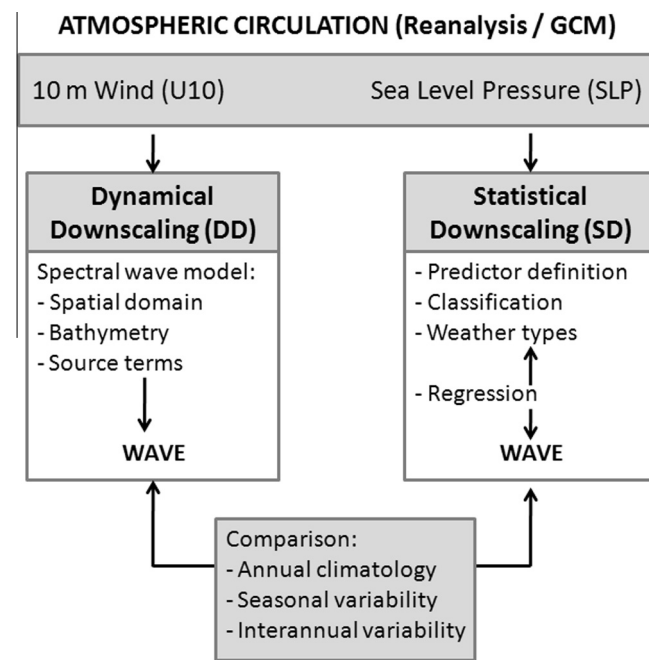


**Fig. 1.** General framework: set-up, application and comparison of the DD and the SD methods.

of a computational mesh from the given time series of wind fields provided by the GCM model. This approach, similar to the numerical hindcasting of wave time series over past decades, takes into account the complex processes of wave generation, propagation and dissipation. In this study, we used the third-generation spectral wave model TOMAWAC (Benoit et al., 1996), which is a module of the Telemac-Mascaret suite of solvers ([www.opentelemac.org](http://www.opentelemac.org)). TOMAWAC solves the wave action density balance equation (Eq. (1)) and simulates the evolution of the directional wave action spectrum,  $N(x, y, k_x, k_y, t)$ , in space and time over oceanic and coastal areas, where  $(x, y)$  and  $(k_x, k_y)$  are the transfer rates in physical and spectral space, respectively; these expressions are obtained from linear wave theory (Benoit et al., 1996):

$$\frac{\partial N}{\partial t} + \frac{\partial(\dot{x}N)}{\partial x} + \frac{\partial(\dot{y}N)}{\partial y} + \frac{\partial(\dot{k}_x N)}{\partial k_x} + \frac{\partial(\dot{k}_y N)}{\partial k_y} = Q(x, y, k_x, k_y, t) \quad (1)$$

On the right-hand-side of Eq. (1), the  $Q$  term embeds several models for wave-related physical processes, such as the wind input, dissipation due to whitecapping, bottom friction and depth-induced breaking, and non-linear wave-wave interactions. The so-called BAJ parameterization (Bidlot et al., 2007) was implemented for the present application to improve the capabilities of the model regarding the wind input and dissipation. In comparison with the combination of Janssen's wind input model (Janssen, 1991) and van der Westhuyzen's whitecapping model (van der Westhuyzen et al., 2007), the BAJ parameterization takes better account of wind sea generation and dissipation through the whitecapping process, particularly in the case of superposition of swells of low frequency and wind sea systems.

The computational domain covers most of the Atlantic Ocean, from 63°S to 80°N, with an unstructured mesh of variable resolution (Fig. 2), allowing reduction of the computational cost required. The mesh includes a total of 13 426 nodes and 22 548 elements and reaches a resolution of up to 20 km along the European coastline and as low as 10 km along the French coastline. At every node of this grid, the wave spectrum is discretized with 32 frequencies, from 0.034 Hz to 0.66 Hz (i.e., periods from 1.5 s to 29.5 s), and

36 directions over the full circle (thus providing an angular resolution of 10°). Bottom elevations are obtained from the GEBCO ([www.gebco.net](http://www.gebco.net)) and Europe (LEGOS, Toulouse, France) bathymetry databases.

ARPEGE-CLIMAT wind field inputs were linearly interpolated in space and linearly in time at every node of the mesh for the four datasets corresponding to the reference period (1961–2000) and the three evaluated scenarios (B1, A1B and A2) for the future period (2061–2100). We chose to directly apply the wind input without any bias adjustment. This choice was motivated by the discussion presented in Hemer et al. (2013a), who found that bivariate quantile bias adjustment of GCM wind fields severely underestimates the monthly 99th percentile of SWH output.

These DD simulations provide four sets of wave climate estimations of a forty-year duration. Due to the required computational cost of approximately 8 h in 24 cores for a one-year simulation run in parallel mode,<sup>1</sup> the 40-year periods were split into 40 simulations of 1 year each (preceded by the last ten days at the end of the previous year as a warm-up period) with a time-step of 300 s.

The DD simulations provide detailed physical results for the sea state, in the form of the full wave spectrum, with a high spatial and temporal resolution. We decided to store the following bulk wave parameters with an hourly resolution at each node of the mesh: significant wave height (SWH), mean wave direction ( $\theta_m$ ), mean wave periods ( $T_{m02}$  and  $T_{m-10}$ ), peak period ( $T_p$ ), angular wave spread (SPD) and wave energy flux (POW).

### 3.2. The statistical downscaling (SD) method

The SD method applied in this study is based on the following concept: at a particular location, the sea state ("predictand Y") is defined as a function,  $Y = F(X)$ , of several atmospheric circulation patterns, referred to as "predictor X". The statistical relationship between the predictand and predictor is built based on the current climatology using atmospheric and sea state databases. Once it is obtained, assuming that the ocean-atmospheric relationships are stationary in the future, we can project predictors from GCM scenarios to simulate the future sea state climate. The following paragraphs detail the main steps of this methodology.

#### 3.2.1. Predictor definition

The quality of the results obtained using the SD method depends on the definition of the predictor. It must be adapted to the predictand location and variables. The more physical the links between the predictor and predictand are, the more valid the assumption of a stationary relationship will be. We assume that the generation area for waves reaching on the French coast can be defined by the region dominated by the most prominent atmospheric circulation pattern in the North Atlantic: the North Atlantic Oscillation (Hurrell et al., 2003). Thus, the selected region was an area from 42.5°W to 10°E and from 35°N to 70°N (see black square in Fig. 2). The variable selected as the predictor for statistical downscaling was SLP because several works have found that a large fraction of the wave height anomalies in the northeast Atlantic are associated with pressure anomalies (Woolf et al., 2002; Wang et al., 2010). Sensitivity tests were applied to determine the best definition of the predictor: a squared SLP gradient adjusted with a latitudinal correction proposed by Wang and Swail (2006) provides a better reproduction of the wave field than the SLP anomaly. As the GCM model of IPCC AR4 shows a mean spatial resolution of approximately 2.1°, the initial resolution of the CFSR SLP was degraded from 0.5° × 0.5° to 2.5° × 2.5°. The

<sup>1</sup> on an IBM machine with a Linux/Debian distribution and the following characteristics: 200 Tflops, 1382 standard nodes (1 standard node = 2 hexa-cores procs) synchronized at 2.93 GHz.

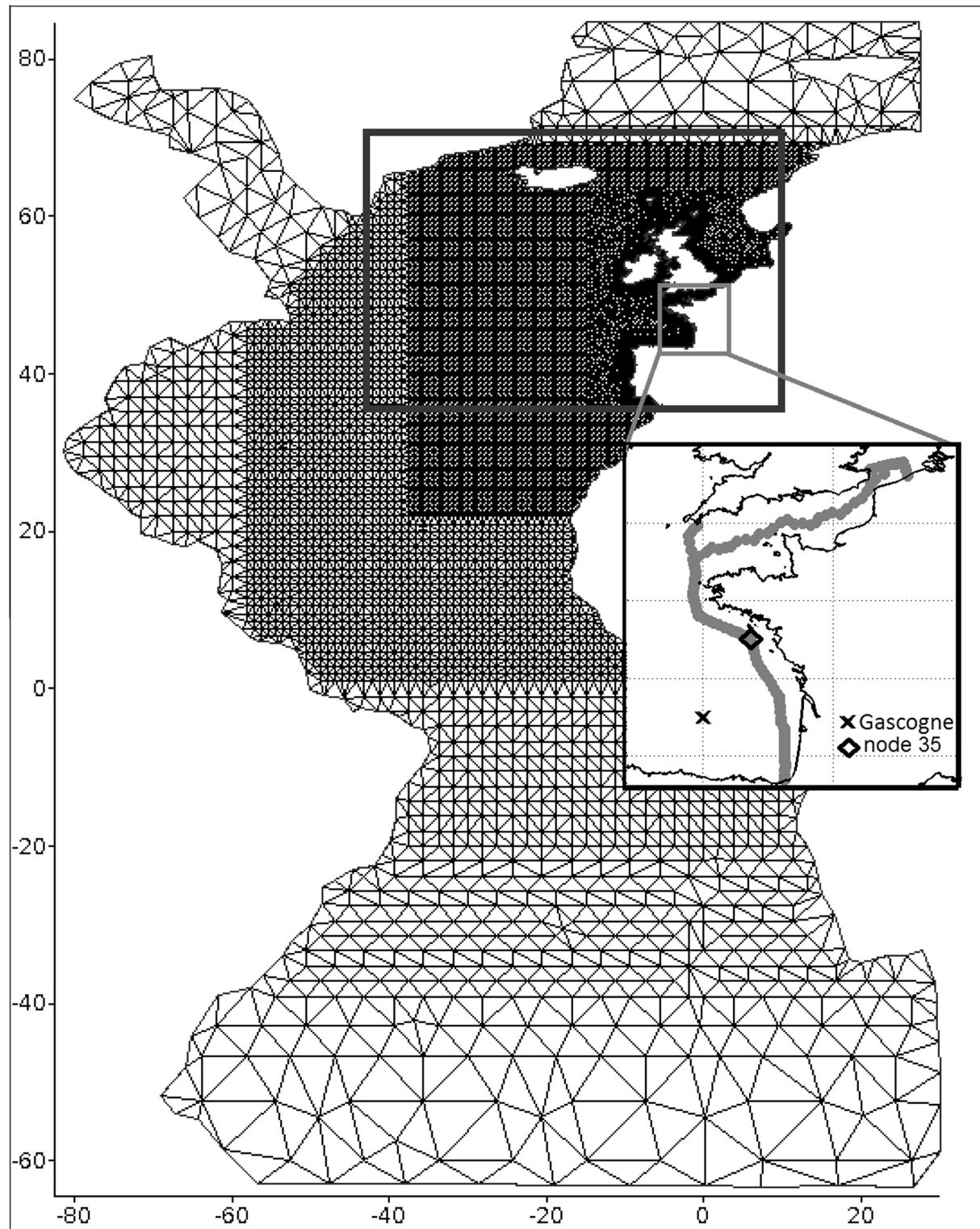


**Fig. 2.** Atlantic mesh of a dynamical wave simulation covering the Atlantic Ocean, defining the French coasts with a 10-km resolution (13 426 nodes and 22 548 elements). The dark rectangle corresponds to the predictor area of the SD method: from 35°N to 70°N and from 42.5°W to 10°E, defined with a spatial resolution of  $2.5^\circ \times 2.5^\circ$ . The coastal zoom shows the locations of the 110 predictand nodes and two particular locations of interest, node 35 (47.07°N, 3.26°W) and the Gascogne buoy (45.14°N, 5°W).

employed predictor from the CFSR SLP database (1979–2009) was the 3-day squared SLP gradient, to allow mid-latitude cyclogenesis situations to be captured. The predictor was standardized with respect to the averaged squared SLP gradient from 1979–2009, which is recommended to reduce the bias related to the model (Wang et al., 2010).

### 3.2.2. Predictor classification

The SD method based on synoptic patterns requires the definition of a sample of  $N$  atmospheric circulation patterns, referred to as weather types and representatives of the northeast Atlantic climate. To reduce the dimensions of the data while retaining the maximum sample variance, a principal component analysis (PCA)

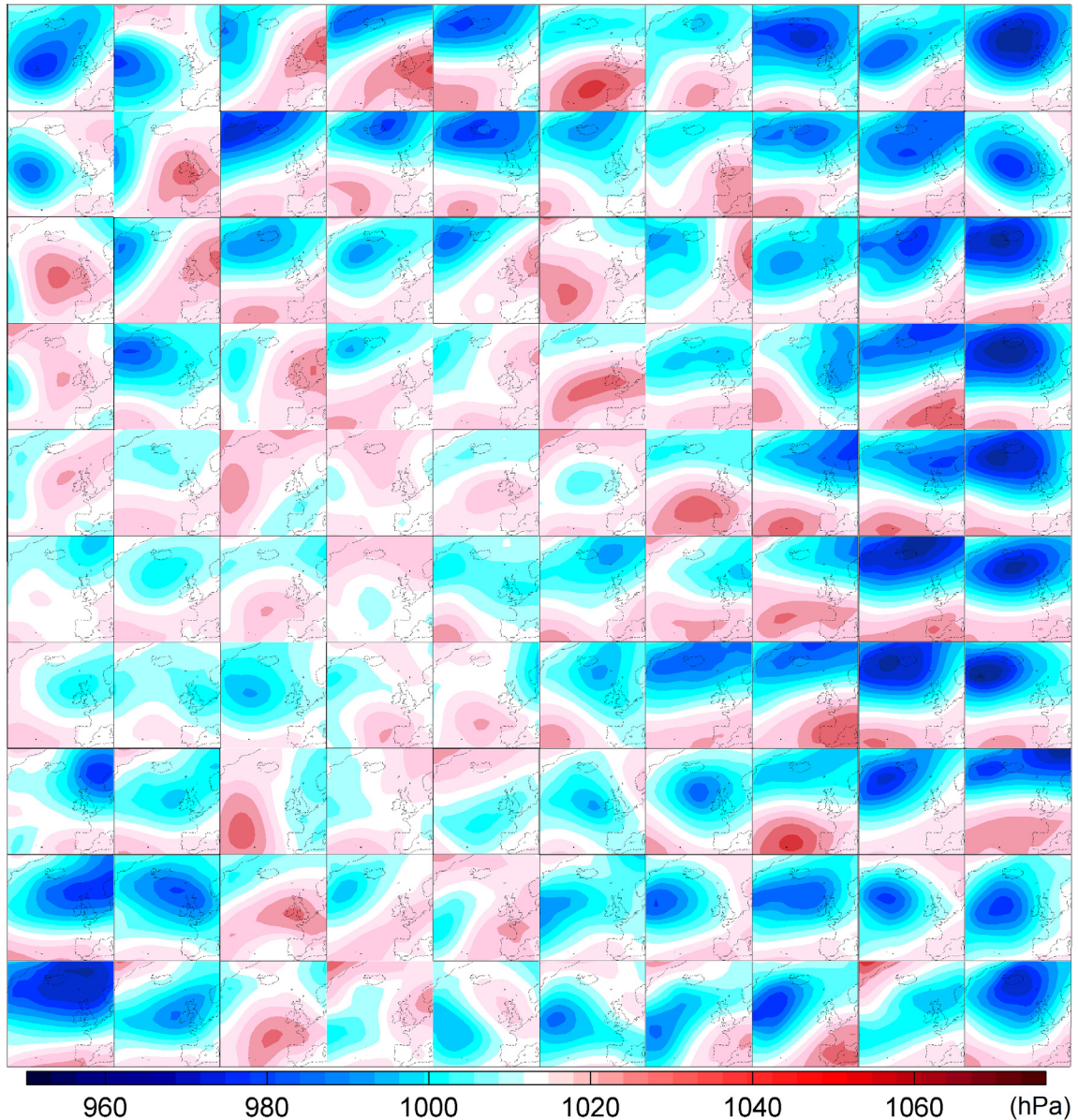


**Fig. 3.** Classification of  $10 \times 10$  SLP (hPa) weather types defined based on the predictor area and associated with the squared SLP gradient classification into  $N = 100$  weather types based on CFSR data (1979–2009).

([Preisendorfer and Mobley, 1988](#)) was first applied to the predictor set. The original set of predictors ( $X(p, t)$ , where  $p$  and  $t$  refer to the spatial and temporal coordinates of the predictors, respectively) was transposed on a new orthogonal basis defined by empirical orthogonal functions,  $e_m(p)$ , and principal components,  $u_m(t)$ , where modes were sorted according to their maximum variance. The first mode concentrated 34.6% of the variability of the initial set. Here, the criterion of preserving 95% of variance was applied; thus, the first sixteen modes were conserved (Eq. (2), where  $M = 16$ ):

$$X(p, t) = \sum_{m=1}^M u_m(t) e_m(p) \quad (2)$$

The K-means clustering algorithm ([Kennard and Stone, 1969; Hastie et al., 2001](#)), initialized by the maximum dissimilarity algorithm (MDA), was applied to the reduced predictor basis, with the aim of identifying a subset of  $N = 100$  clusters to build the

classification. Each cluster corresponds to a group of similar predictors, where linear combinations of them picture a fictive prototype. To build the classification, fictive prototypes were replaced by the nearest real predictor via the minimal Euclidian distance (Eq. (3)). The  $X^{WT}$  prototypes of each group are referred to as weather types (WT) and represent one of the atmospheric circulation patterns over the northeast Atlantic:

$$D = \min \|X^{WT}(p, t) - X^{Predictor}(p, t)\| \quad (3)$$

[Fig. 3](#) shows the classification of the SLP field corresponding to the standardized squared SLP gradient sorted using an algorithm similar to the self-organizing maps ([Kohonen, 2000](#)) over a  $10 \times 10$  grid. The synoptic atmospheric patterns described in [Barry and Perry \(1973\)](#) are illustrated in the classification. The weather types presented in columns 9 and 10 are mainly characterized by low pressure areas centered over the North Atlantic or north of Europe, corresponding to the positive phase of the North

Atlantic Oscillation teleconnection pattern (NAO+), with different degrees of intensity. The negative phase of the NAO is also illustrated in the classification: the last two cells of the sixth column are an example. These patterns are characterized by an anticyclone over Greenland and low pressure crossing the Atlantic Ocean. The NAO teleconnection pattern is one of the most dominant weather types occurring in the North Atlantic. The two phases of the NAO are quite close to the regime patterns identified by Vautard (1990). For example, the NAO+ corresponds to the Zonal regime and the NAO- corresponds to the Greenland Anticyclone. The weather types in row number 8 correspond to an Azores Anticyclone, characterized by high pressure. They are related to the positive phase of the East Atlantic teleconnection pattern (EA+), which is also quite close to the Atlantic Ridge regime. Finally, the calm weather types located in the left-central part of the classification match the Blocking regime in which an Anticyclone covers northern Europe or the Scandinavia region.

Once the classification was obtained based on CFSR data (1979–2009), ARPEGE-CLIMAT SLP fields were built as predictors and distributed into each weather type by means of the minimal Euclidian distance (Eq. (3)). First, the historical period (1970–2000) was used to construct the regression model, and second, the future period (2061–2100) was used to project the future wave climate.

### 3.2.3. Regression model

The construction of the regression model was based on 31 years of ARPEGE-CLIMAT atmospheric data for the present period. ARPEGE-CLIMAT SLP fields from 1970–2000 were calculated as standardized predictors of the 3-day averaged squared SLP gradient. The following variables of the associated sea state database driven according to ARPEGE-CLIMAT wind fields (1970–2000) were extracted with an hourly resolution for the 110 analyzed locations to form the predictand set:

- significant wave height (SWH);
- mean wave period ( $T_{m02}$ );
- mean wave direction ( $\theta_m$ );
- wave energy flux ( $POW$ ).

Predictors were distributed into the cells of the classification according to the nearest Euclidian distance between each predictor and weather type (Eq. (3)), and the corresponding 3-day sea state data were associated with the same weather type. The following local wave predictands were estimated for each weather type to determine the wave climatology:

- mean value and standard deviation of each variable;
- histogram of SWH and  $T_{m02}$ ;



**Fig. 4.** Distribution of  $10 \times 10$  SWH histograms (m) representing the wave climate at Atlantic coastal predictand node number 35 ( $3.26^{\circ}\text{W}$ ,  $47.07^{\circ}\text{N}$ ), built based on the reference period of ARPEGE-CLIMAT (1970–2000). The “n” value indicates the number of hourly SWH data points used to build each histogram reflecting the occurrence of each weather type.

- quantile distribution of SWH;
- joint distribution (SWH,  $T_{m02}$ ) and ( $POW$ ,  $\theta_m$ ).

**Fig. 4** illustrates the distribution of SWH histograms in the weather type classification at a particular node of the Atlantic coastal waters (3.26°W, 47.07°N, grid point number 35, where the water depth is approximately 87.5 m). In addition, the  $n$  value of each cell indicates the number of hourly SWHs used to construct the histogram. It can be observed that the upper right histogram of SWHs, associated with an intensive NAO+ pattern presents higher SWH than the histograms of the eighth column, corresponding to the EA+ mode. Thus, each weather type,  $i$ , is linked to the associated histogram of SWHs by an empirical regression model,  $f_i$ . The resulting general regression model,  $Y = F(X)$ , corresponds to the linear combination of the  $N = 100$  weather type regression models weighted by the probability of occurrence of the weather type,  $p_i$  (Eq. (4)):

$$Y = F(X) = \sum_{i=1}^N p_i f_i(X) \quad (4)$$

### 3.2.4. Wave projection

We assumed the stationary hypothesis in relation to climate dynamics, that is, that the weather type classification remains valid throughout the XXIst century. ARPEGE-CLIMAT SLPs were constructed for the climate change scenarios as standardized 3-day averaged squared SLP gradients and were distributed into the weather type classification by means of the nearest Euclidian distance (Eq. (3)). Future monthly probabilities of occurrence for each

weather type under a climate scenario were estimated and were used to obtain projections of the wave climate. The association of the future monthly probabilities of weather type occurrences and the established statistical relationship between the predictor and predictand for each location were used to project the future wave climate, with monthly time series and wave parameter distributions being generated as results.

### 3.3. Metrics for comparing the SD vs. the DD method

Here, we propose a complete set of comparisons of dynamical and statistical wave projections. Therefore, both annual and seasonal histograms and the mean values of the parameters SWH and  $T_{m02}$  were compared to identify the mean climatology. The joint distributions of (SWH,  $T_{m02}$ ) and ( $POW$ ,  $\theta_m$ ) complete the mean climatology assessment. High percentiles of the SWH are compared throughout the monthly SWH distribution. The monthly and annual time series of the means and standard deviations of the SWH values provide information about the ability of the methods to reproduce the intra-annual and interannual variability of SWH.

The absolute and relative differences in these parameters allow easy spatial visualization to evaluate the ability of the SD method to project future mean values in comparison with the DD method. In addition, the statistical index of the relative entropy,  $RE$  (Eq. (5)), also known as Kullback–Leibler divergence, is used as an indicator of similarity between two sets of data for the histograms and joint distributions of wave parameters:

$$RE\left(\frac{DD}{SD}\right) = \sum P_{SD} \log \frac{P_{DD}}{P_{SD}} \quad (5)$$

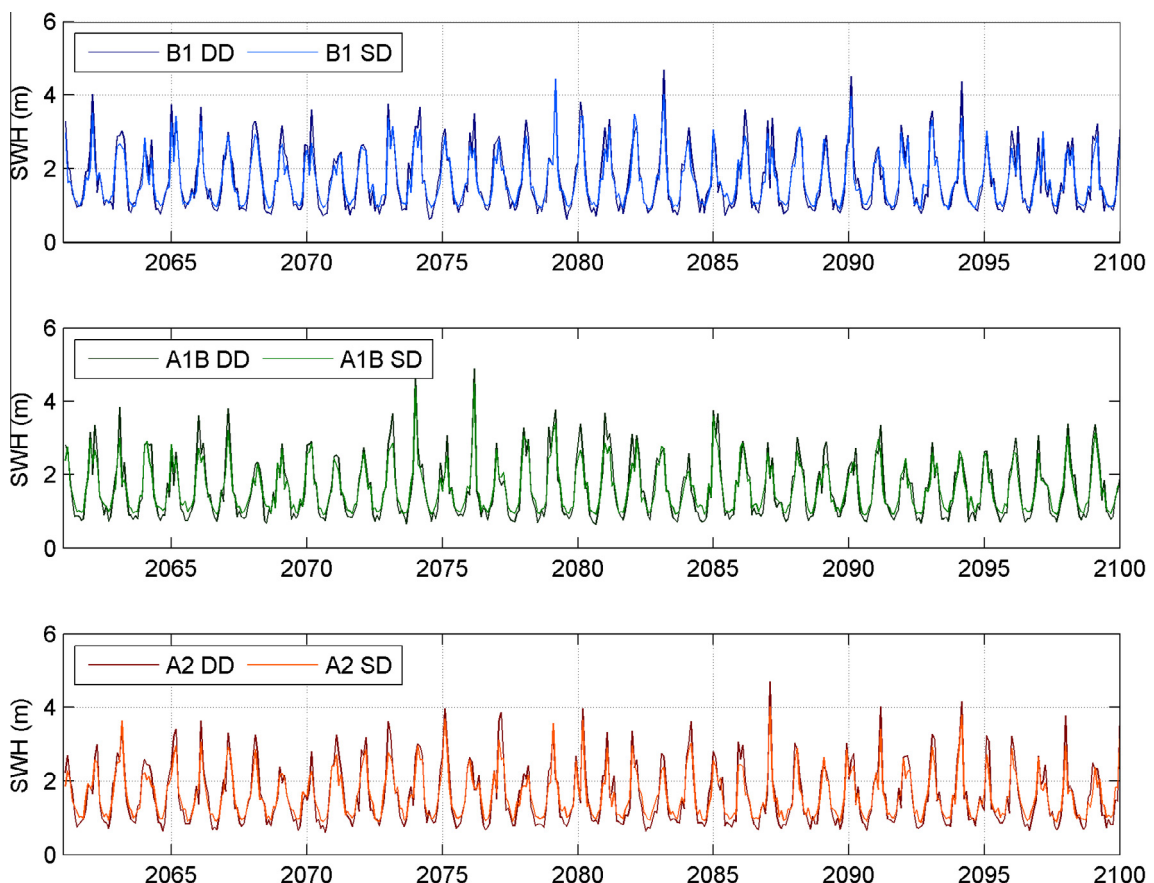


**Fig. 5.** Monthly averaged time series of SWHs (m) from 2061–2100 for the B1, A1B, A2 scenarios of ARPEGE-CLIMAT at node 35 (3.26°W, 47.07°N: Atlantic coastline), plotted in the upper, central and bottom plots, in blue, green and red, respectively. Dark colors correspond to the DD projections, and light colors correspond to the SD projections.

where  $P_{DD}$  and  $P_{SD}$  correspond to the probability of occurrence of dynamical and statistical results for each class, respectively. These indices allow objective evaluations of the differences between the DD and the SD methods to be performed at each location.

#### 4. Results from the dynamical and the statistical downscaling methods

##### 4.1. Annual climatology

The DD and the SD methods were able to simulate the projected wave climate time series under the three climate scenarios along the European Atlantic shoreline from 2061–2100. The monthly time series and statistical distributions of the SWH,  $T_{m02}$ ,  $\theta_m$  and  $POW$  sea state parameters were assessed at 110 locations along the French coast (Fig. 2). A specific coastal location (grid point number 35), in the middle of the French Atlantic coast at  $3.26^\circ\text{W}$ ,  $47.07^\circ\text{N}$ , with a water depth of 87.5 m, was chosen as example of the wave outcomes generated for the 110 locations.

Fig. 5 shows the time series at grid point 35 of the monthly mean SWH values projected via both DD and SD methods under the three climate scenarios. It can be observed that the SD method reproduces the monthly mean SWH values and their within-year variations as well as the DD results. For example, the two methods project similar values of the annual SWH monthly maxima, which vary greatly from one year to another and between the three greenhouse gas emission forcings. These results demonstrate that statistical wave climate projections exhibit the same robustness at the outcomes from dynamical simulations. The main differences between the DD and the SD results are observed during summer. The SD outcomes tend to estimate higher SWH values than the DD monthly mean values during these calm periods. In addition, the DD and the SD methods simulate the peak SWHs during the winter similarly, although the SD method provides slightly lower SWHs for some years.

For the same location, Fig. 6 shows the reconstructed annual joint distribution functions of (SWH,  $T_{m02}$ ) and ( $POW$ ,  $\theta_m$ ) over the period from 2061–2100 and for the A2 scenario. Panels (a) and (d) correspond to the DD method; panels (b) and (e) correspond to the SD method; and panels (c) and (f) show the relative differences between the two methods (DD-SD). It can be observed that the general shapes and probabilities of occurrences of the sea state parameter distributions are similar between the DD and the SD methods. Panels (c) and (f) allow a more detailed comparison. The SD method provides more values for medium-low wave energy (<65 kW/m) propagating eastward (less than a 5% difference with respect to the DD method). On the contrary, a slightly lower probability is observed using the SD method for waves propagating eastward with an energy higher than 70 kW/m, a  $T_{m02}$  of 5 to 10 s and an SWH of 2 to 5 m. According to these results, the SD method is able to reproduce joint distribution functions. Medium-sized waves and swells are very well reproduced, while negligible discrepancies occur for the projections of wind sea and young waves.

To spatially assess and compare the annual wave climatology obtained using the two methods, the  $RE$  index is computed. The index quantifies dissimilarities between joint distribution functions from the DD and SD methods. For example, its value is 0.516 for the (SWH,  $T_{m02}$ ) distribution and 0.381 for the ( $POW$ ,  $\theta_m$ ) distribution at grid point number 35 under the A2 scenario. Fig. 7 illustrates the spatial patterns of the  $RE$  indices estimated under the A2 scenario for the 110 nodes distributed along the French coast. The largest differences in the (SWH,  $T_{m02}$ ) joint distribution are located along the Brittany shoreline, northwest of France. These discrepancies could be due to the poorer ability of the SD method to take into account the propagation and dissipation processes of relevant seas and swells superposed. Surprisingly, the wave projection obtained under the moderate B1 scenario provides higher values of the  $RE$  index on the Brittany coast for the (SWH,  $T_{m02}$ ) joint distribution between the two methods. This

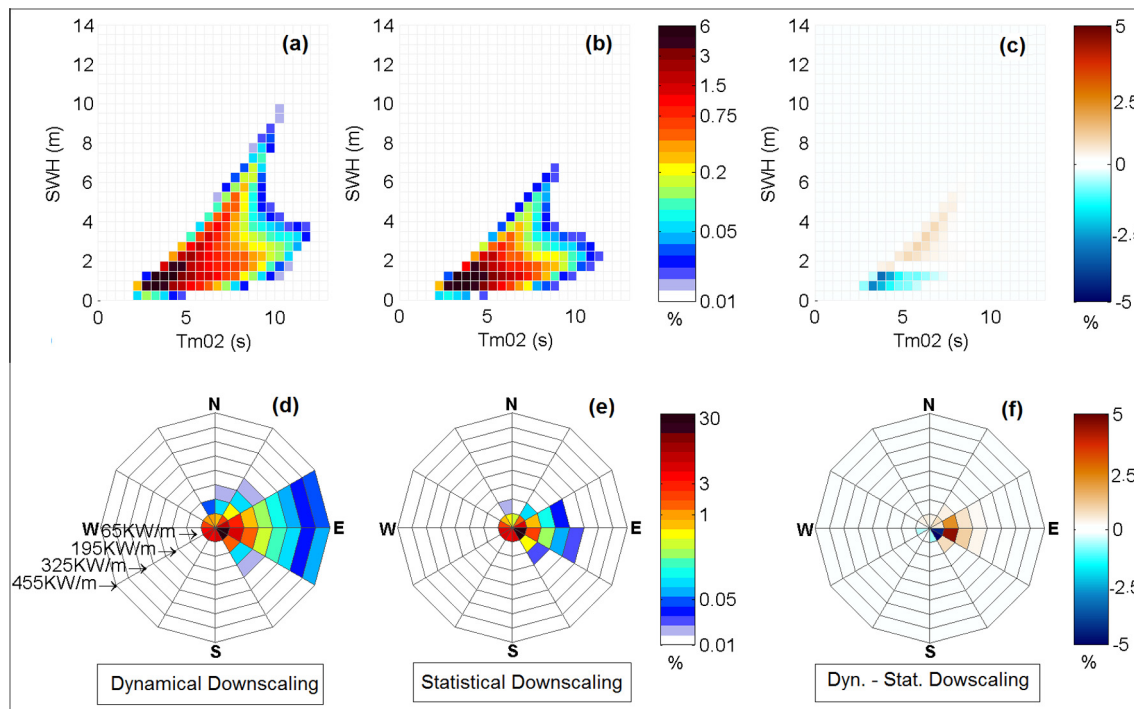


**Fig. 6.** (SWH,  $T_{m02}$ ) joint distributions of the annual climatology at node 35 ( $3.26^\circ\text{W}$ ,  $47.07^\circ\text{N}$ : Atlantic coastline) for (a) the DD method, (b) the SD method and (c) the differences between the two methods (DD-SD), according to A2 scenario of ARPEGE-CLIMAT over the period from 2061–2100. The same layout is used for the ( $POW$ ,  $\theta_m$ ) joint distributions for (d) the DD method, (e) the SD method and (f) the differences between the two methods (DD-SD). The probability functions of (a), (b), (d) and (e) are plotted using a logarithmic color scale, while the distributions of (c) and (f) are plotted with a linear colorscale.

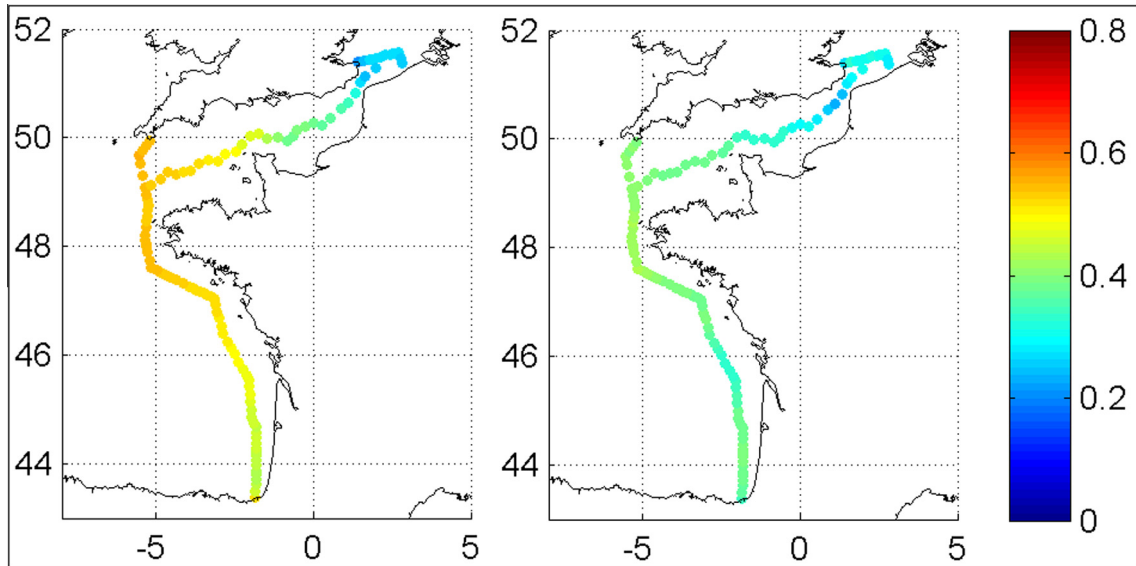


**Fig. 7.** Spatial patterns of relative entropy between the DD and SD methods for the annual joint distributions (SWH,  $T_{m02}$ ) (left) and ( $POW$ ,  $\theta_m$ ) (right) for the A2 scenario of ARPEGE-CLIMAT (2061–2100) along the French coast.

result suggests that the B1 scenario provides the most important fraction of wind sea and young waves along the Brittany coast. The RE index of the ( $POW$ ,  $\theta_m$ ) distribution is low along the whole French coast, with a RE value of approximately 0.4 being obtained at the maximum, while values below 0.3 are observed along the eastern English Channel for the three scenarios (not shown). These findings indicate that the SD method is able to reproduce unidirectional sea states along the Atlantic coast as well as bi-directional sea states proper to the northern French coast.

#### 4.2. Seasonal variability

The seasonal variations along the Atlantic European coast have been well characterized and show a winter-summer pattern

(Young, 1999). In the present study, we sought to analyze the performance of the DD and SD methods in characterizing the projected seasonal variability. The selected approach provides useful information for estimating the uncertainty of evaluations of seasonal changes.

Fig. 8 illustrates the 40-year projected monthly distributions of SWH and the associated standard deviations over the period from 2061–2100 for the three scenarios and the two downscaling methods at grid point number 35. The general variations within a year are similar for the six configurations. The highest means and standard deviations of SWH occur during winter months, from December to February, when means of approximately 2.5 m and a standard deviations of approximately 0.5 m are observed. The lowest values occur during summer months, from June to August,

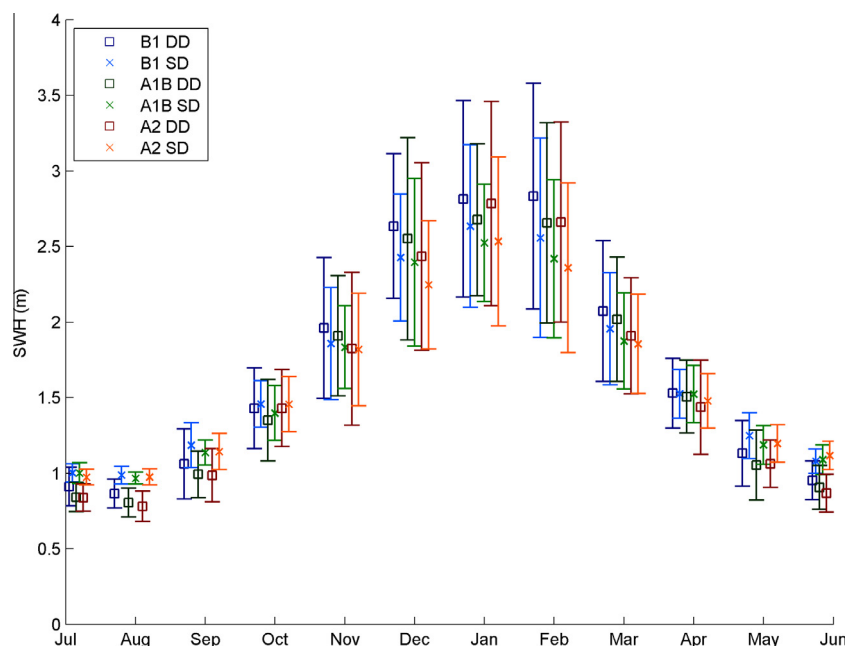


**Fig. 8.** Distributions of the monthly mean values of SWH (m) (with  $\square$  symbols corresponding to the DD method and  $\times$  symbols to the SD method) and the standard deviations of SWH (m) (vertical bars) from 2061–2100 for the B1 (blue), A1B (green), A2 scenarios (red) of ARPEGE-CLIMAT at node 35 (3.26°W, 47.07°N: Atlantic coastline).

when much smaller means and standard deviations, of approximately 1.1 m and 0.15 m, respectively, are recorded. Similar mean SWH values during spring and autumn are obtained for both methods.

Some differences are nevertheless observable between the DD and SD outcomes at this location. The monthly mean SWH values show that the SD approach provides lower and higher means for winter and summer months, respectively, compared with the DD method, as plotted in Fig. 5. In addition, for each month, the SD method provides a lower standard deviation for SWH than the DD method, which means that the SD method suffers a loss of monthly variability. The differences in the mean SWHs between the projection methods are larger than the differences between the scenarios. This suggests that the choice of downscaling method has an impact on the resultant seasonal variability of the projected wave climate of the same order of magnitude as the choice of the greenhouse gas emission scenario.

These differences in the seasonal wave climate projections were evaluated along the French Atlantic coast. Fig. 9 shows the relative differences in seasonal means (top) and standard deviations (bottom) of the SWH between the DD and the SD methods under the A1B scenario for the 110 analyzed grid points over the period from 2061–2100. The largest relative differences in the seasonal mean SWHs for the intermediate climate scenario occur in summer along the French Atlantic coast, reaching values greater than 20%. This difference corresponds to a higher summer mean SWH of approximately 0.15 m under the SD method with respect to the DD method. Nevertheless, in summer, the differences in the eastern part of the English Channel and along the northern French coast are smaller (10 to 5%, i.e., SWH differences of less than 0.05 m). In winter, the differences in mean SWH values are only significant on the French North Atlantic coast, near Brittany. Even though the relative differences in winter are smaller than in summer (up to 10%), they correspond to differences in the mean SWH of approximately 0.20 to 0.25 m in this particular area. Everywhere else, the winter differences in the mean SWH are less than 0.10 m. The seasonal mean SWHs obtained using the DD and the SD methods are almost identical during spring and autumn. The B1 and A2 scenarios provide similar seasonal spatial patterns, though the differences in

the mean SWH values are smaller for the B1 scenario (up to 10%) and are slightly larger for the A2 scenario (up to 25%).

Considering the relative differences in the seasonal standard deviations of SWH between the DD and the SD methods obtained under the A1B scenario, the largest differences are observed east of the English Channel and along the French North Sea coastline during summer and autumn. These areas present relative standard deviation differences of approximately 60%, in contrast to values of 20% along the French Atlantic coastline and west English Channel. The other scenarios show similar spatial patterns, though the differences are more marked in spring and autumn for the A2 scenario and in winter and summer for B1. According to these results, the seasonal variance of SWH is dependent on both the downscaling method and climate scenario.

Figs. 10 and 11 focus on the comparison between the seasonal SWH and  $T_{m02}$  histogram distributions obtained using the DD and the SD methods at grid point 35 for the A2 scenario and for the period from 2061–2100. These figures associate spatial evaluations of the dissimilarity between the distributions for each variable by means of the RE index (Eq. (5)) over the 110 nodes along the French coast. The spatial diagnostic results for SWH and  $T_{m02}$  share the same spatial patterns. All seasons, except for spring, and all scenarios show a boundary around the Cotentin Peninsula (north-westward in the English Channel). It can be observed that the summer and winter wave projections along the Atlantic shoreline show larger differences between the two methods compared with projections along the eastern English Channel coast. In addition, we note the very similar distributions of SWH and  $T_{m02}$  in spring and autumn for all locations. The histograms obtained for grid point number 35 during summer and winter reveal that the DD and SD methods show different behaviors of the lower and upper tails of the SWH and  $T_{m02}$  distributions. The SD results project higher probabilities for larger values of the distributions in summer than the DD method. On the contrary, during winter, the SD results show higher probabilities for the lowest values of the distributions and lower probabilities for the largest values of the distributions compared with the DD method. Nevertheless, we note that the two methods reproduce similar shapes of the seasonal statistical distributions of the sea state parameters.

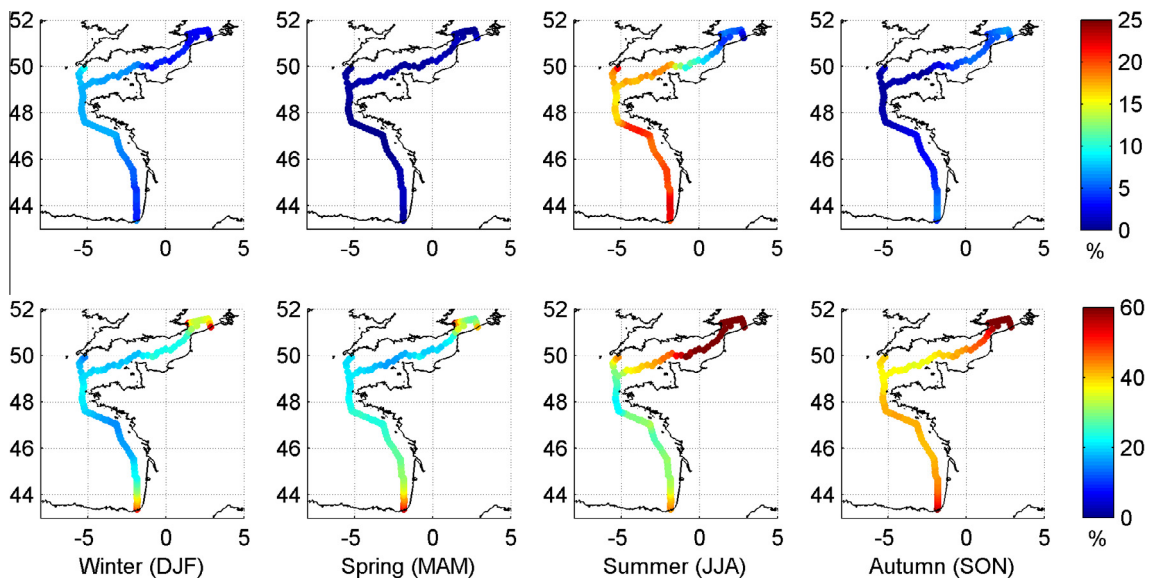


**Fig. 9.** Spatial patterns of the relative differences (%) in the means (top) and standard deviations (bottom) of the seasonal SWH between the DD and the SD projections under the A1B scenario of ARPEGE-CLIMAT, with a monthly resolution (2061–2100) along the French coast.

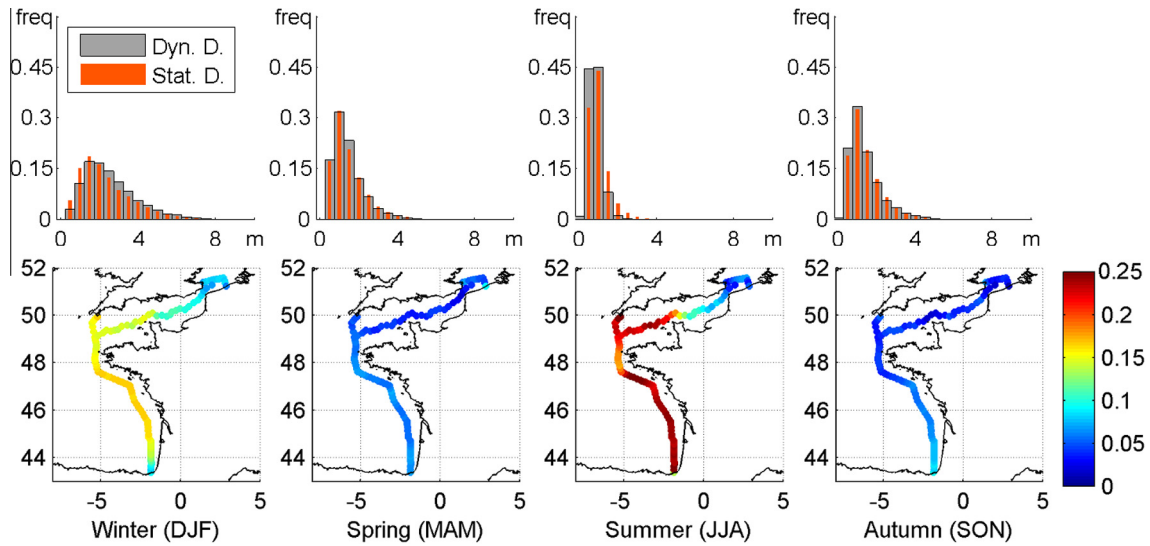


**Fig. 10.** Seasonal histograms of SWH obtained using the DD and SD projections for the A2 scenario of ARPEGE-CLIMAT at node 35 ( $3.26^{\circ}\text{W}$ ,  $47.07^{\circ}\text{N}$ : Atlantic coastline) over the period from 2061–2100 and the seasonal spatial patterns of the associated relative entropy along the French coast.

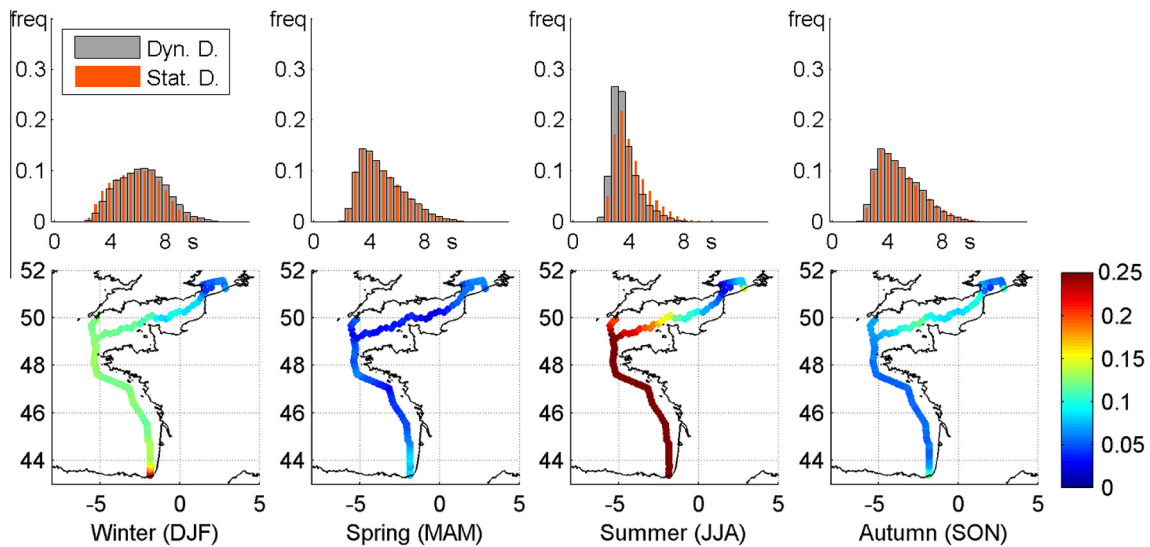


**Fig. 11.** Seasonal histograms of  $T_{m02}$  under the DD and the SD projections for the A2 scenario of ARPEGE-CLIMAT at node 35 ( $3.26^{\circ}\text{W}$ ,  $47.07^{\circ}\text{N}$ : Atlantic coastline) over the period from 2061–2100 and the seasonal spatial patterns of the associated relative entropy along the French coast.

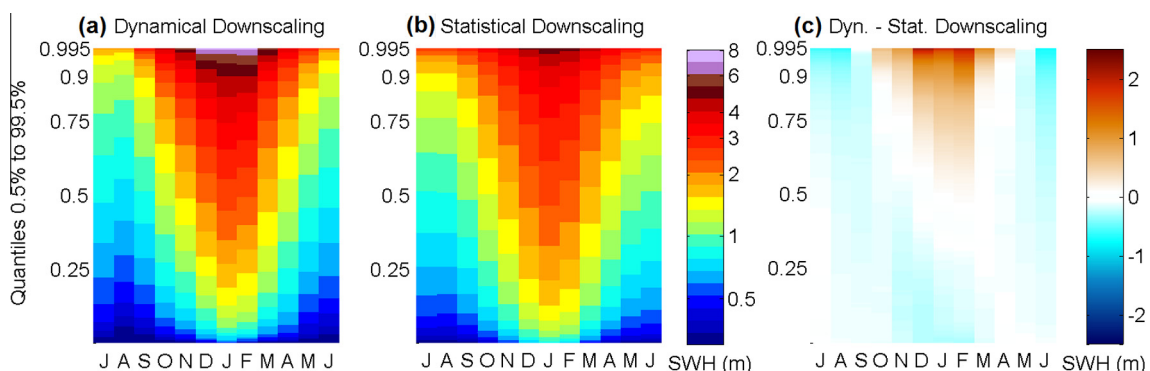


**Fig. 12.** Monthly quantile distributions of SWH under the DD and SD projections for the A2 scenario of ARPEGE-CLIMAT at node 35 ( $3.26^{\circ}\text{W}$ ,  $47.07^{\circ}\text{N}$ : Atlantic coastline) over the period from 2061–2100, where each color corresponds to a SWH value (m). Panel (a) correspond to the DD method, panel (b) to the SD method and panel (c) to the differences between the two methods (DD-SD).

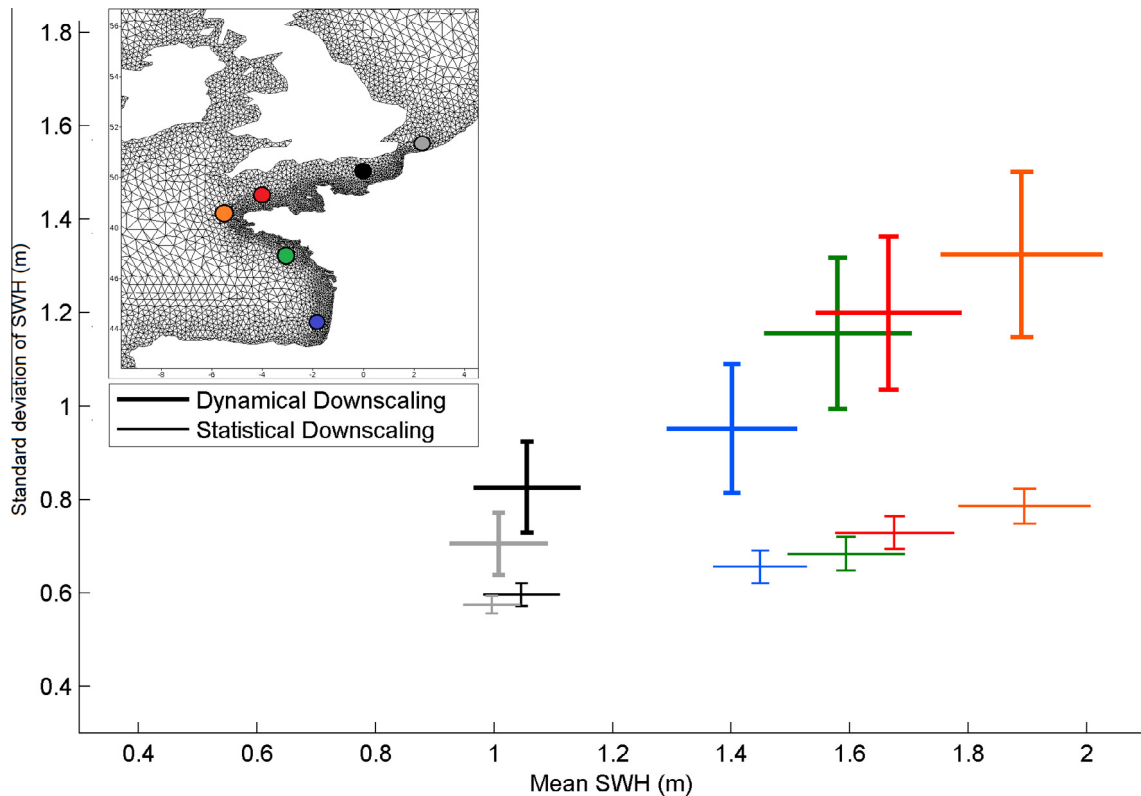


**Fig. 13.** Interannual and intra-annual variability of SWH, represented by crosses, for 6 nodes along the French coast under the DD (in bold) and the SD (in thin) projections of ARPEGE-CLIMAT for the A2 scenario over the period from 2061–2100. The center of each cross corresponds to the mean annual SWH (m) (abscissa) and the mean annual standard deviation (m) (ordinate). Horizontal bars correspond to the standard deviation of the mean annual SWH (m), and the vertical bars correspond to the standard deviation of the annual standard deviations (m). The colors correspond to the 6 locations along the French coastline plotted in the map.

Fig. 12 shows three configurations of the SWH distribution from the 0.5th to the 99.5th percentile at a monthly scale for grid point number 35. The results were built during the period from 2061–2100 for the A2 scenario according to (a) the DD method, (b) the SD method and (c) the differences between the two methods (DD–SD). Panels (a) and (b) show the well-described seasonal variability of the SWH along the Atlantic shoreline. The highest SWHs occur in winter months and were up to 8 m under the DD method and up to 6 m under the SD method. During summer months, the 50th percentile is equal to or lower than 1 m for both methods. The differences between the two methods are more readily observable in panel (c). For example, the SD method provides lower SWH values for the 75th percentile during winter months, by approximately 1 m. This difference in the upper tail of SWH was found across all 110 nodes along the French coast (not shown). The figure also reveals the systematic differences between the distribution tails obtained using the DD and the SD methods. The SD method shows higher SWH values for high percentiles during summer and for lower percentiles during winter (blue areas), and it also shows lower values for high percentiles during winter (red area). Here, it should be considered that the SD method was built to project the mean climate; to better project the upper tail of the wave parameter distributions, a specific SD method should be developed, e.g., as in Izaguirre et al. (2012).

#### 4.3. Interannual variability

As shown in Fig. 5, the obtained wave climate projections present high interannual variability, especially during winter. Comparison of the monthly mean time series of SWHs indicated that the SD approach is able to accurately reproduce mean estimations of

interannual variability. The ability of the SD method to simulate these variations over forty years is shown in Fig. 13, at six locations distributed along the French coast under the A2 scenario. The results are presented using crosses: each cross, characterized by a color and a thickness, corresponds to a location and a method. The abscissa and ordinate axes correspond to the mean SWH values over the period from 2061–2100 and to the mean of the forty annual standard deviations of the SWH, respectively. The vertical bar corresponds to the standard deviation of the forty annual standard deviations and quantifies the variability within a year over the entire evaluated period. The horizontal bar corresponds to the standard deviation of the forty annual means of SWH values, which characterizes the interannual variability.

The abscissas of the crosses nearly converge, except at the southern location. This means that the averaged SWH values obtained over forty years are similar between the two methods, while the SD provides lower SWH mean values for the indicated southern location. In contrast, the ordinates of the SD crosses corresponding to the standard deviation values are all lower compared with those obtained under the DD method. This difference represents a loss of information regarding intra-annual variability under the SD method, as noted in Fig. 9 and demonstrated by Graham et al. (2013). This loss is even greater for nodes characterized by high yearly mean SWH values (along the Brittany coast in particular). Similar information is provided in the vertical bars, which are shorter for the SD projections than for the DD projections. However, the horizontal bars obtained using the two methods are well correlated. This result corresponds to similar standard deviations of yearly SWH means and illustrates the conservation of the interannual variability of SWH when using the SD method with respect to the DD method.

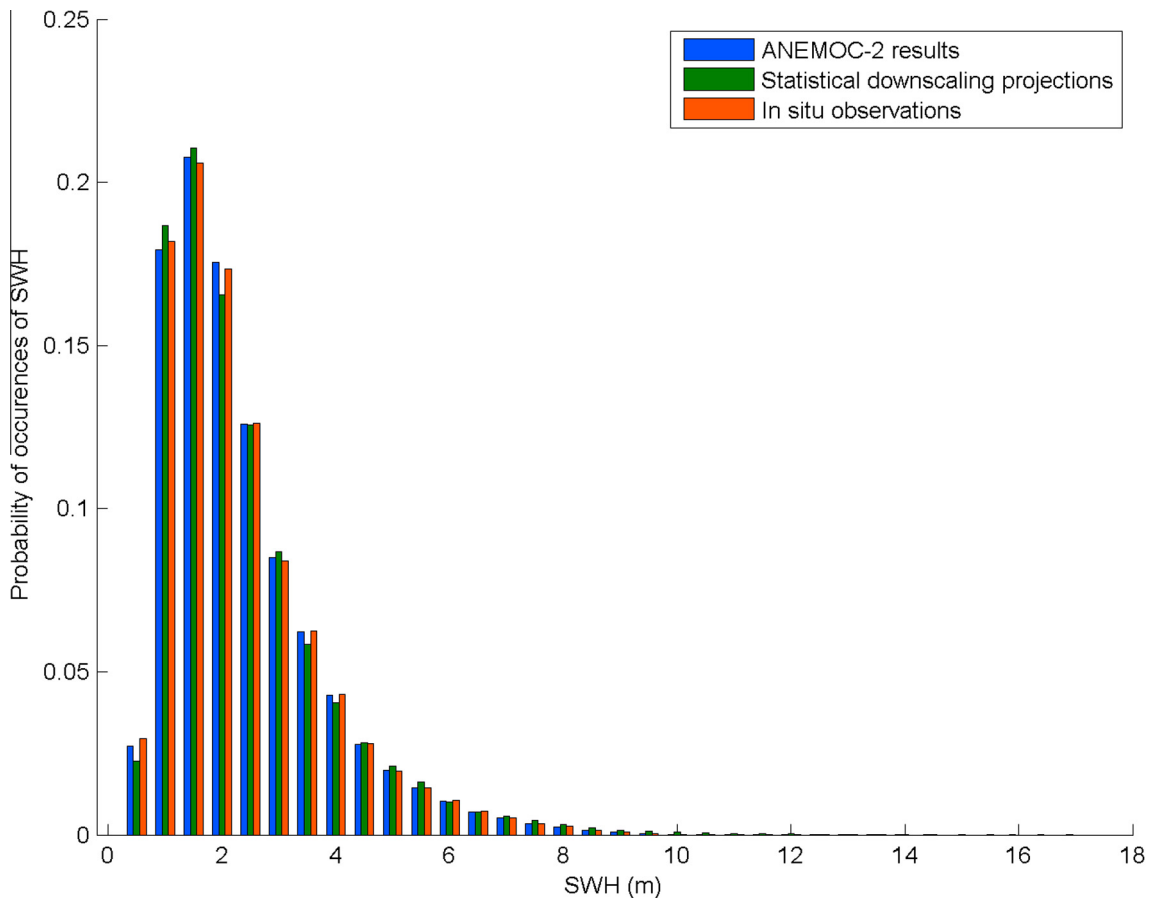


**Fig. 14.** Comparison of the DD and the SD SWH projections (m) at an hourly scale against *in situ* observations at the Gascogne location (45.14°N; 5°W) over the period from 2000–2009.

## 5. Discussions and conclusion

This work compared the distributions of bulk wave parameters (significant wave height, mean wave period, mean wave direction and wave energy flux) obtained using two state-of-the-art downscaling methods applied to one global climate model (GCM) and three greenhouse gas emission scenarios (B1, A1B and A2) (IPCC, 2007). A weather pattern-based statistical downscaling method and a dynamical downscaling method were applied using the ARPEGE-CLIMAT GCM to project the future sea state climate along the French Atlantic, English Channel and North Sea coastlines for the target period of 2061–2100. Under both methods and all three scenarios, wave parameters were compared not only in terms of wave climatology but also considering joint distributions and seasonal and interannual variabilities.

In the general context of estimating the potential impact of climate change on the wave climate, this work aimed to compare the results of two projection methods. The validation step first compared SWH simulations obtained using the two methods for the present wave climate against *in situ* observations performed at the buoy Gascogne located in the Bay of Biscay over the period 2000–2009 (cf. Appendix A) and demonstrated the ability of both methods to estimate the climatology of the SWH, although the DD method provides results that are slightly closer to the observations than the SD method. Therefore, we decided to evaluate the ability of the SD method to model the future sea state with respect to the DD projections, which were considered as reference data. In addition, it was emphasized that uncertainties associated with downscaling methods should be accounted for in estimating the

impact of climate change on seasonal wave variability, in the same manner as model and scenario uncertainties.

We showed that the SD projections are able to reproduce the mean wave climate as well as the DD projections under the three examined climate scenarios, with some differences being observed for high and low values of wave parameters. SWH dynamics at monthly, seasonal and annual scale are well reproduced. In particular, the two methods show a very similar future sea state for spring and autumn, in terms of both mean values and distributions, while the summer and winter projections reveal some differences. The largest of these discrepancies for the A1B scenario correspond to the higher SWH values obtained from the SD projections in summer along the Atlantic coastline and the lower SWH values obtained from the SD projections in winter in the Brittany region with respect to the DD method. In terms of seasonal projections, these differences between the two methods increase from scenario B1 to A1B and from A1B to A2.

The exhaustive comparison of the SD vs the DD methods can contribute to the understanding of the aforementioned differences. First, the analysis of the annual joint distributions of (SWH,  $T_{m02}$ ) and ( $POW$ ,  $\theta_m$ ) indicated that the SD method affects the distributions of wind sea and young waves. Nevertheless, it also shows that developed waves and swells are similarly projected by the two methods, as are uni-directional and multi-directional sea states. Second, the SD method may exhibit limitations in modeling the tails of the wave probability distributions. Comparison of monthly SWH percentiles between the two methods revealed lower values for the SD projections in winter starting from the 75th percentile, reaching approximately 2 m for the 99th percentile along the

French Atlantic coastline. Finally, these differences are linked by the loss of monthly variability under the SD method in comparison with the DD method.

Nevertheless, the estimates of the future mean wave climate obtained using the SD method based on weather type classification match the estimates obtained using the DD method, at least for the dominant features, but with a much lower computational cost. Similar results were obtained for seasonal mean values, joint distributions and future interannual variability. However, some improvements of the SD method could be considered to enhance the modeling of wind seas and energetic sea states. These improvements could concern the definition of the predictor, such as an increase in the spatial resolution or the inclusion of a model dedicated to extreme values in the SD method to better capture the upper tail of the SWH distribution.

Finally, considering the limitations and advantages of both downscaling methods, the authors recommend that the advantages of each technique should be exploited. The SD method could be applied with an ensemble of GCMs and scenarios to estimate the potential impact of climate change on the mean wave climatology and the associated uncertainties. Application of the DD method could also complete the estimation of the possible impact of climate change on more energetic sea state conditions and quantify the downscaling uncertainties inherent to the projection of the future wave climate.

## Acknowledgments

This work was carried out using ARPEGE-CLIMAT data and *in situ* observations, for which Météo-France is greatly acknowledged. The author also thanks NOAA for providing the CFSR data. This work was partially funded by the French ANRT (CIFRE PhD grant 2010/0653) and the “IMAR21” project (CTM2010-15009) of the Spanish Government. The authors also acknowledge the three reviewers of the manuscript for their useful comments, which helped to improve the article.

## Appendix A. Validation of the DD and the SD methods for the present climate

To highlight the robustness of the DD and the SD methods in projecting the future wave climate, both methods were first applied and validated for the present climate using *in situ* observations made at the Gascogne buoy (45.14°N; 5°W, see Fig. 2) in the Bay of Biscay over the period from 2000–2009.

The DD method was previously applied for the present climate to build the hindcast wave database ANEMOC-2 (Laugel et al., 2014), covering the Atlantic Ocean and focusing on the French Coast (see domain and mesh in Fig. 2). To achieve this, the method described in Section 3.1 was applied over the period from 1979–2010 using 10 m wind fields obtained from CFSR reanalysis (Saha et al., 2010), with a spatial resolution of 0.312° × 0.312° and a temporal resolution of one hour. Thus, the spectral simulations conducted over 32 years resulted in detailed physical modeling of the wave parameters in the northeast Atlantic Ocean from which the SWH at the Gascogne buoy location was extracted.

On the other hand, the SD method has also been applied to the present climate to be compared with the same *in situ* observations conducted over the period from 2000–2009. To estimate the ability of the SD method to project the wave climate independent of the learning period, the following steps of the method were applied. First, the SD method was performed as described in Section 3.2, using the CFSR sea level pressure field and ANEMOC-2 wave parameters as input data, over a learning period of 21 years from 1979–1999. This step resulted in the construction of a 21-year

CFSR classification and a specific regression model corresponding to this period and to the Gascogne buoy location. Second, the CFSR predictor (3-day averaged squared SLP gradient with a 2.5° resolution over the area from 35°N to 70°N and from 42.5°W to 10°E) from 2000–2009 was distributed based on the weather type classification described above, which provided new probabilities of occurrence for each weather type. Then, based on this regression model, the SD method was able to project the wave parameter at a monthly scale or the wave climatology at an hourly scale over the period from 2000–2009 at the location of interest.

In this context, validation of both methods for the present climate against *in situ* observations is possible. For example, Fig. 14 shows histograms for the SWH at the Gascogne buoy location during the period from 2000–2009, built with an hourly resolution based on (i) ANEMOC-2 results (DD method), (ii) SD projections and (iii) and *in situ* observations. It can be observed that the SWH distributions are quite similar for the three sets of data. However, the DD method provides a slightly better estimation of the SWH observed at the Gascogne location than the SD method. Furthermore, we emphasize that the SD method used for the validation step has a learning period of only 21 years, in comparison with the method applied to estimate the future climate in the core of the article, for which the period was 31 years, which means that the 31-year SD method could provide an even more accurate estimation of the wave climate.

In conclusion, this validation step for both the DD and SD methods against *in situ* observations confirmed the ability of both methods to reproduce the local wave climate. This gives us some confidence in applying and comparing the SD and DD methods for the future climate using the ARPEGE-CLIMAT GCM as input data.

## References

- Barry, R.G., Perry, A.H., 1973. *Synoptic Climatology, Methods and Applications*. Methuen and Co Ltd, London.
- Benoit, M., Marcos, F., Becq, F., 1996. Development of a third generation shallow-water wave model with unstructured spatial meshing. In: 25th International Conference on Coastal Engineering. ASCE, Orlando, FL USA, pp. 465–478.
- Bidlot, J.-R., Janssen, P., Abdalla, S., 2007. A revised formulation of ocean wave dissipation and its model impact. ECMWF Tech. Rep. Memo., Reading, UK.
- Boé, J., Terray, L., Martin, E., Habets, F., 2009. Projected changes in components of the hydrological cycle in French river basins during the 21st century. *Water Resour. Res.* 45, W08426.
- Charles, E., Idier, D., Delecluse, P., Déqué, M., LeCozannet, G., 2012. Climate change impact on waves in the Bay of Biscay France. *Ocean Dyn.* 62, 831–848.
- Espejo, A., Camus, P., Losada, I.J., Mendez, F.J., 2014. Spectral ocean wave climate variability based on atmospheric circulation patterns. *J. Phys. Oceanogr.* <http://dx.doi.org/10.1175/JPO-D-13-0276.1>.
- Graham, N.E., Cayan, D.R., Bromirski, P.D., Flick, R.E., 2013. Multi-model projections of twenty-first century North Pacific winter wave climate under the IPCC A2 scenario. *Clim. Dyn.* 40, 1335–1360.
- Hastie, T., Tibshirani, R., Friedman, J., 2001. *The Elements of Statistical Learning*. Springer, New-York.
- Hemer, M.A., Katzley, J., Trenham, C.E., 2013a. Global dynamical projections of surface ocean wave climate for a future high greenhouse gas emission scenario. *Ocean Modell.* 70, 221–245.
- Hemer, M.A., Fan, Y., Mori, N., Semedo, A., Wang, X.L., 2013b. Projected changes in wave climate from a multi-model ensemble. *Nat. Clim. Change* 3, 471–476.
- Hurrell, J.W., Kushnir, Y., Ottersen, G., Visbeck, M. (Eds.), 2003. *The North Atlantic Oscillation: Climate Significance and Environmental Impact*, Geophysical Monograph Series, vol. 134, 2003, p. 279.
- IPCC, 2007. An assessment of the intergovernmental panel of climate change, Synthesis Report.
- Izaguirre, C., Menendez, M., Camus, P., Méndez, F.J., Minguez, R., Losada, I.J., 2012. Exploring the interannual variability of extreme wave climate in the Northeast Atlantic Ocean. *Ocean Modell.* 59, 31–40.
- Janssen, P.A.E.M., 1991. Quasi-linear theory of wind-wave generation applied to wave forecasting. *J. Phys. Oceanogr.* 21, 1631–1642.
- Kennard, R.W., Stone, L.A., 1969. Computer aided design experiments. *Technometrics* 11, 137–148.
- Kohonen, T., 2000. *Self-Organizing Maps*, third ed. Springer-Verlag, Berlin.
- Laugel, A., Tiberi-Wadier, A.-L., Benoit, M., Mattarolo, G., 2014. ANEMOC-2 Atlantique et Méditerranée: calibration et validation de deux nouvelles bases d'états de mer construites par simulations numériques rétrospectives sur 1979–

2010. In: XIII<sup>e</sup> Conférence Journées Nationales Génie Côtier Génie Civil, Dunkirk, France (in French).
- Morellato, D., Benoit, M., Tiberi-Wadier, A.-L., 2010. Simulations des états de mer dans l'océan Atlantique de 1960 à 2100 pour trois scénarios de changement climatique. In: Journées "Impacts du changement climatique sur les risques côtiers", Orléans, France, BRGM (in French).
- Mori, N., Yasuda, T., Mase, H., Tom, T., Oku, Y., 2010. Projection of extreme wave climate change under global warming. *Hydrol. Res. Lett.* 4, 15–19.
- Mori, N., Shimura, T., Yasuda, T., Mase, H., 2013. Multi-model climate projections of ocean surface variables under different climate scenarios – future change of wave, sea level and wind. *Ocean Eng.* 71, 122–129.
- Najac, J., Boé, J., Terray, L., 2008. A multi-model ensemble approach for assessment of climate change impact on surface winds in France. *Clim. Dyn.* 32, 615–634.
- Preisendorfer, R.W., Mobley, C.D., 1988. Principal component analysis in meteorology and oceanography. *Developments in Atmospheric Science*. Elsevier, Amsterdam.
- Saha, S., Moorthi, S., Pan, H.-L., Wu, X., Wang, J., Nadiga, S., Tripp, P., Kistler, R., Woollen, J., Behringer, D., Liu, H., Stokes, D., Grumbine, R., Gayno, G., Wang, J., Hou, Y.-T., Chuang, H.-Y., Juang, H.-M.H., Sela, J., Iredell, M., Treadon, R., Kleist, D., van Delst, P., Keyser, D., Derber, J., Ek, M., Meng, J., Wei, H., Yang, R., Lord, S., van den Dool, H., Kumar, A., Wang, W., Long, C., Chelliah, M., Xue, Y., Huang, B., Schemm, J.-K., Ebisuzaki, W., Lin, R., Xie, P., Chen, M., Zhou, S., Higgins, W., Zou, C.-Z., Liu, Q., Chen, Y., Cucurull, L., Reynolds, R.W., Rutledge, G., Goldberg, M., 2010. The NCEP climate forecast system reanalysis. *Bull. Am. Meteorol. Soc.* 91, 1015–1057.
- Salas-Mélia, D., Chauvin, F., Déqué, M., Douville, H., Guérémy, J.F., Marquet, P., Planton, S., Royer, J.F., Tyteca, S., 2005. Description and validation of CNRM-CM3 global coupled climate model. *Tech. Rep. Note de centre GMGEC 103*, CNRM, Météo-France, Toulouse, France.
- Semedo, A., Weisse, R., Behrens, A., Sterl, A., Bengtsson, L., Günther, H., 2013. Projection of global wave climate change toward the end of the twenty-first century. *J. Clim.* 26, 8269–8288.
- Tisseuil, C., Vrac, M., Lek, S., Wade, A.J., 2010. Statistical downscaling of river flows. *J. Hydrol.* 385, 279–291.
- van der Westhuysen, A.J., Zijlema, M., Battjes, J.A., 2007. Nonlinear saturation-based whitecapping dissipation in SWAN for deep and shallow water. *Coastal Eng.* 54, 151–170.
- Vautard, R., 1990. Multiple weather regimes over the North Atlantic: analysis of precursors and successors. *Mon. Weather Rev.* 118, 2056–2081.
- Wang, X.L., Swail, V.R., 2006. Climate change signal and uncertainty in projections of ocean wave heights. *Clim. Dyn.* 26, 109–126.
- Wang, X.L., Zwiers, F.W., Swail, V.R., 2004. North Atlantic ocean wave climate change scenarios for the twenty-first century. *J. Clim.* 17, 2368–2383.
- Wang, X.L., Swail, V.R., Cox, A., 2010. Dynamical versus statistical downscaling methods for ocean wave heights. *Int. J. Climatol.* 30, 317–332.
- Weisse, R., von Storch, H., Callies, U., Chrastansky, A., Feser, F., Grabemann, I., Günther, H., Pluess, A., Stoye, T., Tellkamp, J., Winterfeld, J., Woth, K., 2008. Regional meteo-marine reanalyses and climate change projections: Results for Northern Europe and potentials for coastal and offshore applications. *Bull. Am. Meteorol. Soc.* 90, 849–860.
- Wilby, R.L., Charles, S.P., Zorita, E., Timbal, B., Whetton, P., Mearns, L.O., 2004. Guidelines for use of climate scenarios developed from statistical downscaling methods. Supporting material of the IPCC.
- Woolf, D.K., Challenor, P.G., Cotton, P.D., 2002. Variability and predictability of the North Atlantic wave climate. *J. Geophys. Res.* 107, 9–1–9–14.
- Young, I.R., 1999. Seasonal variability of the global ocean wind and wave climate. *Int. J. Climatol.* 19, 931–950.